# Relaxation Processes in Nonlinear Optical Polymers: A Comparative Study

**Philippe Prêtre,† Urs Meier, Urs Stalder, Christian Bosshard, and Peter Günter***

*Institute of Quantum Electronics, Swiss Federal Institute of Technology, CH-8093 Zürich, Switzerland*

**Philip Kaatz**

*Department of Physics, University of Nevada—Las Vegas, Las Vegas, Nevada 89154*

**Christoph Weder, Peter Neuenschwander, and Ulrich W. Suter**

*Institute for Polymers, Swiss Federal Institute of Technology, CH-8092 Zürich, Switzerland*

*Received September 15, 1997; Revised Manuscript Received December 29, 1997*

ABSTRACT: Relaxation processes in nonlinear optical (NLO) polymers with glass transition temperatures in the range of 125 °C < $T_g$ < 176 °C have been studied. The relaxational mechanisms of these side- and main-chain polymers have been investigated above and below the glass transition by second-harmonic decay, dielectric relaxation, and differential scanning calorimetry measurements, and the results obtained have been compared with a variety of nonlinear optical polymer systems cited in the literature. The *nonexponential* relaxation in both the time and frequency domain was modeled by the Kohlrausch−Williams−Watts function whereas the *nonlinear* relaxational behavior of these polymers was modeled in terms of the Tool−Narayanaswamy description of the glassy state using the Adam−Gibbs expression for the relaxation time. This procedure allows for the nonlinear extension of the liquid equilibrium state behavior into and below the glass transition region with an accurate prediction of the relaxation times over more than 15 orders of magnitude in time. Time−temperature scaling of the relaxation times with respect to $T_g/T$ as the relevant scaling parameter is observed below the glass transition. The effect of annealing was investigated using differential scanning calorimetry with the result that a single set of parameters is sufficient to describe a wide range of thermal histories with as well as without annealing. Optimum annealing temperatures/annealing times for best orientational stability in NLO polymers were calculated according to the same relaxation scheme.

## 1. Introduction

Understanding relaxational processes in nonlinear optical (NLO) polymeric materials is of critical importance in order to evaluate the long-term stability of poled polymers that are in development for potential electro-optic applications. Previous work has demonstrated that the basic concepts in developing poled polymers as NLO materials are well-understood.[1−6] Although this class of polymers was primarily intended to be used in frequency-doubling devices for the conversion of near-IR radiation into the blue wavelength region, second-harmonic generation (SHG) as the underlying fundamental process has emerged as a new diagnostic tool for studying relaxation mechanisms primarily below the glass transition of these materials (at relaxation times in the order of hours up to months). However, it was shown recently that SHG can serve as a probe for the entire range of relaxation times above and below the glass transition.[7]

The physical origin of the glass transition is primarily associated with the cooperative motions of large-scale molecular segments of the polymer.[8] Thus, to prevent reorientation of the NLO chromophores, the formation of a glassy state at relatively high temperatures is an essential requirement for stabilizing the required noncentrosymmetric orientation in polymeric NLO materials. Furthermore, there has been considerable discussion in the literature as to whether universal scaling of relaxation times measured by SHG exists below the glass transition and, if so, what is the appropriate description of the scaling relation.[9,10] Recently, some of us developed a model of the glass transition that provides an explanation of most of the observed thermal behavior of glassy polymers as probed by differential scanning calorimetry (DSC) measurements.[11] The model was also shown to be useful for the calculation of relaxation times of the NLO effect due to electric-field poling. In the present work, we compare the reported relaxation data in a variety of NLO polymer systems described in the literature (glass transition temperatures $T_g$ in the range from 94 to 350 °C) with our own corresponding relaxational measurements of the side- and main-chain polymers above and below $T_g$.

The model was developed by using a correspondence to other phenomenological theories of the glass transition in order to provide a better understanding of the temperature dependence of relaxational processes in NLO polymers. Widely used phenomenological descriptions of glassy materials such as the Fulcher−Tammann−Hesse[12] (FTH) equation:

$$\tau = A \exp\left(\frac{B}{T - T_2}\right) \tag{1.1}$$

with $\tau$ the relaxation time, $T$ the temperature, and $A$, $B$, and $T_2$ the FTH parameters. Another widely used phenomenological expression is the Williams−Landel−

† Current address: Department of Electrical and Comp. Engineering, University of California, Davis, CA 95616.

S0024-9297(97)01362-4 CCC: $15.00 
Published on Web 02/27/1998

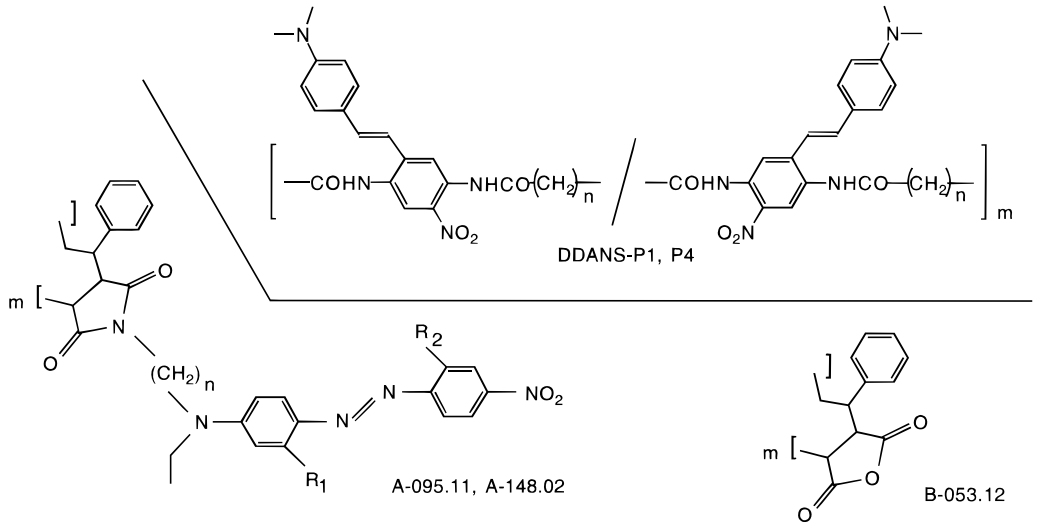


**Figure 1.** Chemical structures of the nonlinear optical main- and side-chain polymers studied in this work.

Ferry[13] (WLF) equation:

$$\log \frac{\tau}{\tau_g} = \frac{-C_1^g(T - T_g)}{C_2^g + T - T_g} \tag{1.2}$$

with $\tau_g$ the relaxation time at the glass transition temperature $T_g$, and $C_2^g$ and $C_1^g$ the WLF parameters. These two equations are not independent descriptions of relaxation near the glass transition as the WLF equation can easily be rewritten in an FTH form as[14−16]

$$\log \frac{\tau}{\tau_g} = -C_1^g + \frac{C_1^g C_2^g}{(T - T_2)} \tag{1.3}$$

if $T_2$ is defined as $T_2 = T_g - C_2^g$. These equations provide a quantitative description of relaxation for most glassy materials in the liquid state above the glass transition temperature. By incorporating a WLF parametrization of the Tool−Narayanaswamy description of the glass transition,[17,18] we are able to extend the characterization of glassy materials to temperatures below $T_g$. This model thus provides a description of the global temperature relaxation behavior of glasses both above, below, and through the glass transition. Using this model of the glass transition, we are then able to predict the temperature and processing conditions (cooling rates, annealing times, temperatures, etc.) needed to optimize the relaxational properties of poled NLO glassy polymers.

## 2. Nonlinear Optical Side- and Main-Chain Polymers

The chemical structures of the polymers studied in this work are shown in Figure 1. In the case of the side-chain polymers, alkyl amino functionalized NLO azo chromophores, with the various substitution patterns shown in Table 1, were attached via a two- or three-carbon spacer linkage to an alternating styrene−maleic anhydride copolymer. For the main-chain polymers a series of polyamides based on the bifunctional chromophore DDANS [2′,5′-diamino-4-(dimethylamino)-4′-nitrostilbene] and aliphatic diacid chlorides with a different number of methylene groups were used (polymer DDANS−P1 and DDANS−P4). Details of the synthesis of all polymers were reported elsewhere.[19,20] The two polymers denoted by A-095.11 and A-148.02 with the chromophores indicated in Table 1 and the precursor polymer B-053.12 were chosen for the annealing studies described in this work. In previous communications, we have reported measurements characterizing the linear and nonlinear optical properties and the relaxation behavior of these polymers.[11,20−22]

**Table 1. Nomenclature, Azo Dye Substitution Patterns, and Glass Transition Temperatures for the Polyamide Main-Chain and Polyimide Side-Chain Polymers Discussed in This Paper**

| polymer | $n$ | $R_1$ | $R_2$ | $T_g$ [°C] |
|---|---|---|---|---|
| DDANS-P1 | 12 | | | 125 |
| DDANS-P4 | 6 | | | 176 |
| B-053.12 | | | | 213 |
| A-095.11 | 3 | $CH_3$ | H | 137 |
| A-148.02 | 2 | H | H | 172 |

## 3. Theoretical Discussion

**(a) Tool−Narayanaswamy Model of the Glass Transition.** Hodge has given a recent review of the main features of enthalpic relaxation and recovery in glassy materials.[23] The analysis for the quantitative calculation of enthalpic relaxation in glassy materials is usually based on studies by Tool[17] and Narayanaswamy[18] which we will denote the TN (Tool-Narayanaswamy) procedure. Using a minor modification of Scherer's[24] application of the Adam−Gibbs formulation[8] of the configurational entropy of the corresponding relaxing segments, Hodge[25] has derived an expression for the structural relaxation time $\tau$:

$$\tau = \tau_0 \exp\left(\frac{B}{T(1 - T_2/T_f)}\right) \tag{3.1}$$

where $B$ is an activation energy divided by the gas constant $R$, $T$ is the temperature, and $\tau_0$ is a pre-exponential time parameter. The temperature $T_2$ in this formulation is described by the temperature where the configurational entropy vanishes. The use of a fictive temperature, $T_f$, as a measure of the extent of deviation from thermal equilibrium provides a description of the relaxational behavior of glassy materials below $T_g$. Using the TN procedure, the fictive temperature is

calculated from the previous thermal history of temperature steps d$T'$ by using the following expression:

$$T_f(T) = T_0 + \int_{T_0}^{T} T'\left\{1 - \exp\left[-\left(\int_{T'}^{T} \frac{dT''}{q\tau}\right)^b\right]\right\} \quad (3.2)$$

where $q = dT''/dt$ is the heating/cooling rate and $T_0$ is an arbitrary reference temperature above the glass transition temperature. The Kohlrausch−Williams−Watts (KWW) function provides the nonexponentiality in the TN procedure as described by Moynihan et al.[26] Our algorithm evaluates $T_f$ numerically in a manner similar to Hodge and Berens.[27]

Recently, we have shown that the TN formalism can be usefully interpreted in terms of the WLF parameters describing glassy state behavior.[11] In this previous paper, extensive parameter correlation studies of enthalpic relaxation measurements clearly indicated that the pre-exponential time parameter within the TN formalism could be written as $\tau_0 = \tau_g \exp(-2.303C_1^g)$, where $\tau_g$ is the relaxation time at the glass transition temperature. This relation also follows from consideration of eqs 1.1−1.3 and is also given in other discussions of the glass transition.[28] From this expression for $\tau_0$ we find it useful to describe the global relaxation behavior both above and below $T_g$ using the TN model with WLF parameters $C_1^g$ and $C_2^g$ taken from Fulcher−Tammann−Hesse (FTH) fits to dielectric (DK) data from temperatures above $T_g$. Using the WLF parameters, eq 3.1 can be written as[11]

$$\log R_\tau^g = -C_1^g + \frac{C_1^g C_2^g}{T(1 - T_2/T_f)} \quad (3.3)$$

where $R_\tau^g = \tau/\tau_g$, $\tau$, and $\tau_g$ are the structural relaxation times at temperature $T$ and at the glass transition temperature, respectively. Equation 3.3 is equivalent to the WLF equation in the form of eq 1.3 at temperatures above $T_g$, if $T_2$ is again written as $T_2 = T_g - C_2^g$.

Annealing is incorporated into the TN model by rewriting the integrand of eq 3.1 in the time domain during the annealing time $t_a$ and annealing at temperature $T_a$:

$$T_f(T) = T_0 + \int_{T_0}^{T_a} dT'\left\{1 - \exp\left[-\left(\int_{T'}^{T_a} \frac{dT''}{q\tau} + \int_0^{t_a} \frac{dt}{\tau} + \int_{T_a}^{T} \frac{dT''}{q\tau}\right)^b\right]\right\} + \int_{T_a}^{T} dT'\left\{1 - \exp\left[-\left(\int_{T'}^{T} \frac{dT''}{q\tau}\right)^b\right]\right\} \quad (3.4)$$

where the three integral terms in the first integral over T′ of eq 3.4 give the relaxation before, during, and after annealing, respectively, of the temperature steps d$T'$ that occur before $T_a$, while the second integral over T′ describes the relaxation of the temperature steps d$T'$ that occurred after the annealing process.

Figure 2 illustrates the evolution of the fictive temperature for a thermal cycle starting above the glass transition and cooling ($q = -5/10$ K/min) to far below $T_g$ and subsequently heating the sample back above $T_g$. The fictive temperatures for both an unannealed and an annealed (1 h at 400 K) sample of polymer A-095.11 are illustrated in the figure, as calculated from eqs 3.2 and 3.4.

**(b) Determination of the Glass Transition/Scaling Law for Relaxation Times.** For the interpretation of eq 3.3 and for the derivation of the scaling of

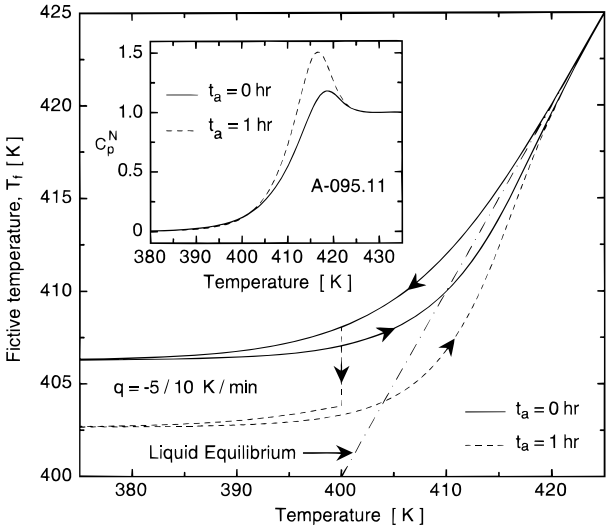


**Figure 2.** The evolution of the fictive temperature for a thermal cycle of the NLO polymer A-095.11 starting above $T_g$, cooling to well below $T_g$, and subsequently heating back above $T_g$. Both unannealed (solid line) and annealed (dashed line, 1 h at 400 K) cycles are shown. The cooling/heating rate for both cycles is $q = -5/10$ K/min. The corresponding normalized DSC heat capacity curves, $C_p^N$, are shown in the inset. Note that the absolute limit of the fictive temperature in cooling or annealing processes is given by the temperature indicated by the liquid equilibrium line or $T_2$, whichever is higher.

relaxation times, it is necessary to consider how the glass transition temperature $T_g$ is defined in the context of our work. Basically, there are two options discussed in the literature: (1) The midpoint definition from DSC measurements, where $C_p^N = 0.5$[23] (see section 5a). (2) $T_g = T_{f'}$, the final fictive temperature achieved in cooling processes.[29,30] The first is by far the most practical choice from an experimentalist's point-of-view and will therefore be used throughout this paper, as we wish to compare our results with those previously published. Both (1) and (2), however, present problems in our version of modeling the glass transition by the TN procedure with a *fixed* set of parameters for *all* thermal histories, since the value for $T_g$ depends on the previous thermal history in these definitions. For example, using DSC parameters for polymer A-095.11 in Table 2, the $T_g$'s defined by (1) and (2) range from 395 to 415 K and from 388 to 398 K, respectively, for cooling rates $-0.01$ K/min $> q > -100$ K/min. We note, however, that suitable parameters can be found from both definitions such that the observed enthalpic response (DSC curve) for a specific thermal history can be equally well-fitted from either definition. Although the use of $T_g$ as an enthalpic variable introduces these complications in the TN formalism, quite often the glass transition may be the only enthalpic parameter known for a wide variety of polymers. The glass transition thus forms a useful point of reference in discussing the limiting temperature behavior of the structural relaxation time of glasses as described by eq 3.3.

At low temperature, $T_f \rightarrow T_{f'}$; and eq 3.3 gives

$$\log R_\tau^g = -C_1^g + \frac{T_{f'}}{T} \frac{C_1^g C_2^g}{(T_{f'} - T_2)} \quad (3.5)$$

and with $\delta T \equiv T_g - T_{f'}$ (according to definition 1) above this reduces to

**Table 2. WLF Parameters and Fragility Values Based on Enthalpic (DSC) and Dielectric Data (DK) for Selected Polymers and Other Glassy Materials[a]**

| material | method | $C_1^g$ | $C_2^g$[K] | $T_2$ [K] | $T_g$[K] | $\tau_g$ [s] | $b$ | $m_{WLF}$ | $m$ | $q$ [K/min] | ref |
|---|---|---|---|---|---|---|---|---|---|---|---|
| PS-DR1 | DK | 10.5 | 35 | 332 | 367 | 2.8 | 0.24 | 100 | 90 | −5/+20 | TW |
| A-095.11 | DK | 11.8 | 54 | 356 | 410 | 20 | 0.44 | 92 | 67 | −5/+20 | 11 |
| A-148.02 | DK | 11.6 | 55 | 389 | 444 | 15 | 0.52 | 92 | 73 | −5/+20 | 11 |
| DDANS-P1 | DK | 12.0 | 49 | 349 | 398 | 4.7 | 0.38 | 97 | 83 | −5/+20 | TW |
| A-095.11 | DSC | 48.9 | 260 | 150 | 410 | 54 | 0.44 | 77 | 65 | −5/+20 | 11 |
| A-148.02 | DSC | 43.1 | 294 | 150 | 444 | 42 | 0.52 | 65 | 57 | −5/+20 | 11 |
| B-053.12 | DSC | 65.3 | 266 | 220 | 486 | 40 | 0.44 | 119 | 90 | −20/+20 | TW |
| DDANS-P1 | DSC | 44.3 | 228 | 170 | 398 | 1.0 | 0.38 | 77 | 75 | −5/+20 | TW |
| PVAc | DSC | 30.7 | 88 | 225 | 313 | 66 | 0.55 | 109 | 63 | −20/+20 | 31 |
| PVC | DSC | 27.6 | 41 | 320 | 361 | 51 | 0.28 | 243 | 135 | −20/+20 | 31 |
| PS | DSC | 45.6 | 163 | 210 | 373 | 100 | 0.74 | 104 | 68 | −10/+10 | 31 |
| PS | DSC | 29.3 | 113 | 260 | 373 | 56 | 0.54 | 97 | 63 | −10/+10 | 31 |
| PMMA | DSC | 26.1 | 57 | 325 | 382 | 110 | 0.34 | 175 | 99 | −10/+10 | 31 |
| PC | DSC | 32.1 | 95 | 325 | 420 | 40 | 0.54 | 142 | 90 | −10/+10 | 31 |
| glycerol | DSC | 16.0 | 59 | 134 | 193 | 16 | 0.51 | 52 | 36 | −20/+20 | 32 |
| glycerol | DSC | 20.0 | 73 | 120 | 193 | 16 | 0.51 | 53 | 38 | −20/+20 | 32 |
| NBS710 | DSC | 10.0 | 351 | 494 | 845 | $5.2 \times 10^{-5}$ | 0.63 | 24 |  | −20/+20 | 24 |
| NBS710 | DSC | 9.89 | 291 | 554 | 845 | 38 | 0.68 | 29 | 22 | −20/+20 | 11 |
| NBS711 | DSC | 17.0 | 482 | 248 | 730 | 71 | 0.67 | 26 | 22 | −20/+20 | 33 |
| $B_2O_3$ | DSC | 18.1 | 278 | 286 | 564 | $9.3 \times 10^{+6}$ | 0.65 | 37 |  | −10/+10 | 32, 33 |
| $B_2O_3$ | DSC | 17.4 | 279 | 285 | 564 | 82 | 0.70 | 35 | 27 | −10/+10 | 11 |
| $P_2O_5$ | DSC | 12.4 | 455 | 150 | 605 | 130 | 0.77 | 16 | 15 | −10/+10 | 34 |
| $Pb(PO_3)_2$ | DSC | 32.1 | 253 | 350 | 603 | 110 | 0.64 | 77 | 53 | −10/+10 | 34 |
| ZBLA | DSC | 33.5 | 162 | 425 | 587 | $7.1 \times 10^{+6}$ | 0.46 | 121 |  | −10/+10 | 32, 33 |
| ZBLA | DSC | 27.6 | 162 | 425 | 587 | 52 | 0.54 | 100 | 68 | −10/+10 | 11 |

[a] The glass transition $T_g$ is defined by the midpoint definition, $C_p^N = 0.5$. TW: this work.

$$\log R_\tau^g \approx -C_1^g + C_1^g(1+\xi)\frac{T_g}{T} \qquad (3.6)$$

with $\xi = (T_2/(T_g - \delta T))(\delta T/C_2^g)$. Whereas if we choose $T_g = T_{f'}$ (definition 2) above, eq 3.3 gives

$$\log R_\tau^g = -C_1^g + C_1^g\left(\frac{T_g}{T}\right) = C_1^g\left(\frac{T_g - T}{T}\right) \qquad (3.7)$$

as described previously.[11,21] Note that with the change in $T_g$ in eq 3.7 from eq 3.6, the corresponding WLF parameters will be different for the two definitions. The dependence of $C_1^g$ and $C_2^g$ with respect to $T_g$ has been given previously by Ferry.[15] Equation 3.7 predicts Arrhenius behavior below $T_g$ with the reduced temperature $T_g/T$ as the natural scaling parameter. However, since glass transition temperatures are usually given by the midpoint definition (1), eq 3.6 provides an equivalent picture of the scaling behavior with $C_1^g\xi$ being the apparent excess slope in the Arrhenius line compared to eq 3.7. The activation energy in both cases, however, is $\ln(10)RC_1^gT_g$ with $R$ the gas constant and where the glass transition temperature is defined by $T_g = T_{f'}$. Figure 3 shows a scaled plot of $\log R_\tau^g$ versus $T_g/T$ for several glass formers, NBS 711, glycerol, the NLO polymer A-095.11, and PMMA, using the midpoint definition for $T_g$, $C_p^N = 0.5$ from DSC measurements and WLF parameters from Table 2.[11,24,31−34]

At high temperatures, $T_f \rightarrow T$ and eq 3.3 reduces to the FTH equation written with the WLF parameters as given in eq 1.3:

$$\log R_\tau^g = -C_1^g + \frac{C_1^g C_2^g}{T - T_2} \qquad (3.8)$$

where the high-temperature limit is $\log R_\tau^g = -C_1^g$. Note that the Arrhenius line given by eqs 3.6 or 3.7 extrapolate to the same limit at high temperatures as that given by eq 3.8.

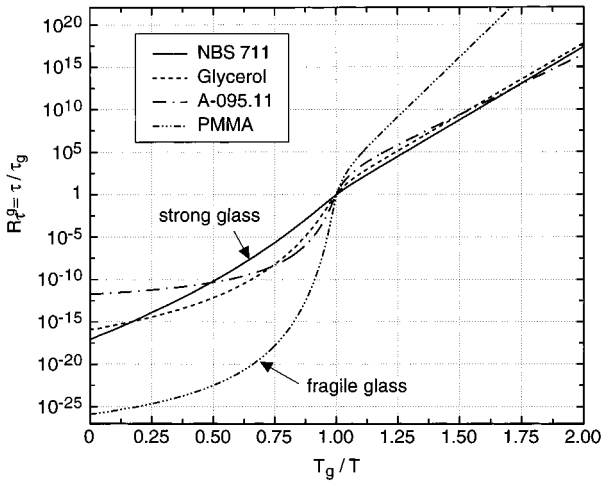


**Figure 3.** Relaxation time scaling showing a plot of $R_\tau^g$ vs $T_g/T$ for NBS 711, glycerol, the NLO polymer A-095.11, and poly(methyl methacrylate) (PMMA), using the midpoint definition 1) of the glass transition from DSC measurements, $C_p^N = 0.5$. The WLF parameters for A-095.11 were taken from dielectric (DK) measurements above $T_g$, while the parameters for the other glasses were taken from fits to DSC data (Table 2). Note that the experimentally accessible temperature range is typically only from $0.8 < T_g/T < 1.3$. The high ($\log R_\tau^g = -C_1^g$) temperature limit and the Arrhenius temperature dependence below $T_g$, with slope $C_1^g\xi$ (see text), are consequently difficult to assess unequivocally from experimental measurements.

**(c) Aspects of "Strong/Fragile" Glass Classification.** The "strong/fragile" classification of liquids/glasses has provided a means of characterizing a number of similarities and differences between various glass-forming materials.[35−39] The description of strong/fragile behavior refers to glass formers with small/large configurational heat capacities and therefore small/large structural changes near the glass transition. To date, most of the discussion has been confined to the liquid-state behavior above $T_g$ (see however Hodge[40] for a

recent critique). As previously mentioned, our formulation of the TN model of the glass transition provides a characterization of glassy materials both above and below $T_g$. The fragility concept provides a means of characterizing the *scaled* relaxation behavior of glasses between the high/low-temperature extremes, namely in the temperature range of the glass transition.

The "steepness index"[41] or the "fragility",[42] $m$, near $T_g$ can in general be defined as the effective activation enthalpy at $T_g$:[36,42,43]

$$m = \frac{\partial \log R_\tau^g}{\partial (T_g/T)}\Big|_{T=T_g} \tag{3.9}$$

The fragility values calculated in this way with log $R_\tau^g$ defined as in eq 3.3 are compiled in Table 2. Most other work, however, uses the FTH or the equivalent WLF description of glassy state relaxation above $T_g$ to evaluate the fragility.[36,42,44,45] Following eq 3.8 in terms of the WLF parameters, the fragility is then given by

$$m_{WLF} = C_1^g \frac{T_g}{C_2^g} = C_1^g \frac{T_g}{T_g - T_2} \tag{3.10}$$

For "strong" glass-forming liquids, $m$ is low as $T_2 \to 0$, yielding a minimum fragility value of $m_{min} = C_1^g$, this being true for both eqs 3.9 and 3.10. In this case, Arrhenius behavior is observed with slope $C_1^g$ over the entire temperature range, this being consistent with eqs 3.6 or 3.7 below the glass transition and also with the high-temperature limit given by eq 3.8 (see, for example, the curve for the strong glass former NBS 711 in Figure 3).

However, for fragile glass-forming liquids with fragilities $m \gg C_1^g$, the values $m_{WLF}$ from eq 3.10 will be less accurate than the numerically calculated values from the TN eqs 3.3 and 3.9 given in Table 2 as $m$, since eq 3.8 does not account for the transition to glassy behavior with slope $C_1^g$ at low (below $T_g$) temperatures. The WLF parameters for PMMA, for example, yield a $m_{WLF}$ value of 175 whereas the numerically calculated value via eqs 3.3 and 3.9 of $m$ is 99 using the same WLF parameters. Equation 3.10 gives similar results to those found in Table 1 from Böhmer et al.,[36] who also define the slope near $T_g$ by the FTH equation, and is equivalent to an expression used previously by others.[40,44,45]

## 4. Results and Discussion

**(a) Scaling in Nonlinear Optical Polymers.** Equation 3.7 indicates that the primary or α-relaxation process in glasses should have an Arrhenius temperature dependence below the glass transition. In addition, from the "universality" of the WLF parameter $C_1^g$ (see also section 4b), one might expect normalized relaxation time ratios to scale with the scaling parameters $T_g/T$ or $(T_g - T)/T$.

We compare now the scaling behavior of our polymers with some typical representatives of NLO polymers cited in the literature: Lophine 1/Ultem guest−host systems,[9,46] DR1/PS,[47] a guest−host system, where also SHG relaxation measurements above $T_g$ were performed, statistical and block main-chain copolymers based on DDANS, 4-(bis(2-hydroxyethyl)amino)benzaldehyde-1,1-diphenylhydrazone (BBDH) and adipic acid,[48,49] high $T_g$ polyimides (PI-1, 2, 3),[50] and an interpenetrating network (IPN) NLO polymer.[51] In Figure 4a, the results for guest−host and side-chain polymers are shown together with Arrhenius, FTH, and TN traces. These traces have been calculated using the

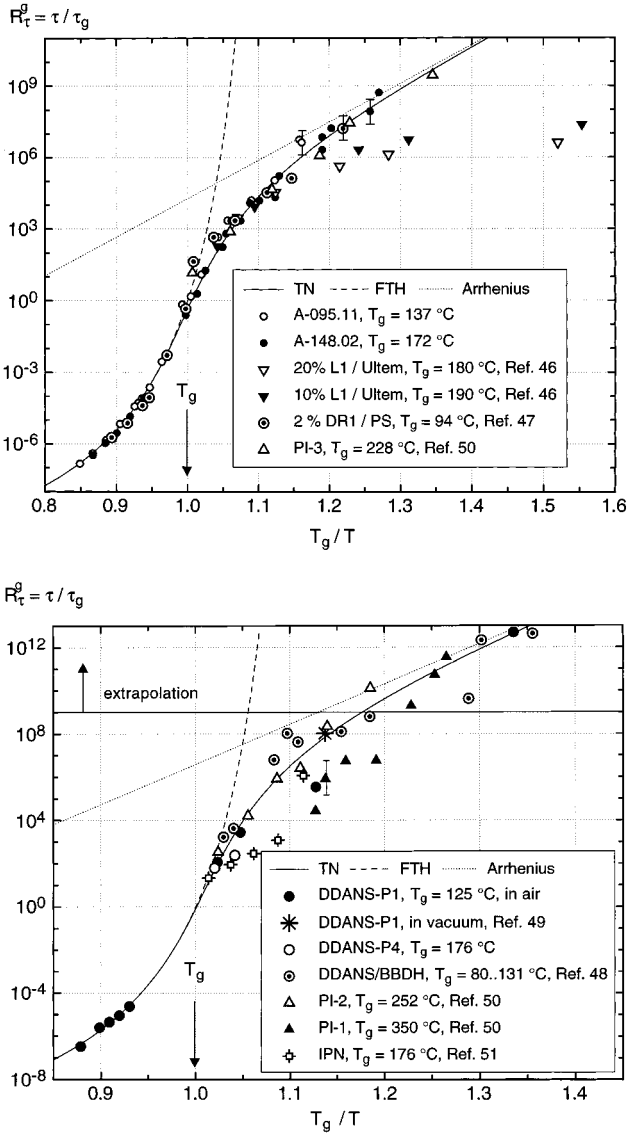


**Figure 4.** (a) Temperature scaling of normalized dielectric loss and SHG relaxation times with respect to the scaling variable $T_g/T$ of typical side-chain and guest-host NLO polymers cited in the literature. Points below $T_g$ represent SHG relaxation data. Data above $T_g$ originate from dielectric relaxation measurements except for the guest−host system 2% DR1 in polystyrene (PS) where the entire relaxation times spectrum was recorded from SHG decay studies. Curves were calculated using the TN procedure with WLF parameters from dielectric (DK) measurements for the polyimide side-chain polymer A095.11 ($b = 0.21$, $q = -5$ K/min). The influence of the structure on relaxation becomes obvious slightly above $T_g$ where the TN line deviates from the FTH line. A remarkable temperature scaling is found among the side-chain polymers (note that the large range of glass transition temperatures). Guest−host systems deviate toward shorter relaxation times at lower scaled temperatures with increasing guest molecule concentration. (b) As Figure 4a for main-chain and interpenetrating network NLO polymers. Curves were calculated using the TN procedure with WLF parameters from dielectric (DK) measurements for the polyamide side-chain polymer DDANS-P1 ($b = 0.19$, $q = -0.32$ K/min). Relaxation times that exceed actual measurement times by more than 3 orders of magnitude are subject to large uncertainties and have to be seen rather as an extrapolation.

TN procedure with WLF parameters of A-095.11 determined by dielectric (DK) relaxation measurements above $T_g$ (see Table 2). Figure 4b illustrates the relaxation times for main-chain and IPN polymers.

To determine the ratio $R_\tau^g = \tau/\tau_g$, the relaxation time at the glass transition temperature $\tau_g$, has to be known for a given $T_g$. Usually, values for $\tau_g$ are around 1−100 s.[11] For the Lophine 1/Ultem guest−host systems, $\tau_g$ was estimated from Figure 3 of ref 46 to be 25 s, whereas a FTH fit to the DR1/PS data gave $\tau_g = 2.8$ s for $T_g = 94$ °C. A least-squares fit (on a logarithmic time scale) of the relaxation times for the high $T_g$ polyimide PI-3 to the TN trace yielded $\tau_g = 2.0$ s. Since the FTH eq 3.8 gives relaxation times for a fully relaxed system, experimentally determined ratios $R_\tau^g$ below $T_g$ should always be lower than the FTH ratio at a given temperature. Now, assuming $R_\tau^g$ to be given by the FTH equation for the data point closest to the respective $T_g$ of PI-2 and the IPN polymer, $\tau_g$ was taken to be 5 and 550 s, respectively. For PI-1, $\tau_g$ was assumed to be 1 s, since no further information was available. For all our polymers $\tau_g$ was determined with FTH fits to dielectric relaxation data with $T_g$ determined by the midpoint definition (1) of normalized DSC curves (see Figure 10).

The side-chain polyimide PI-3 shows excellent scaling with our side-chain polyimides. However, it is obvious from Figure 4a that guest−host systems deviate strongly from the expected TN behavior at lower temperatures. Relaxation times for these guest−host systems seem to level off at around $10^7-10^8$ s. Because of the low dye loading in the case of DR1/PS, no "guest−host behavior" is seen for the measured temperatures. The good agreement above $T_g$ with our polymers is due to the similar WLF parameters for this polymer (see Table 2).

All the main-chain-type polymers (DDANS, PI-1, and DDANS/BBDH) tend to have a somewhat steeper Arrhenius slope than the side-chain systems. Comparing WLF parameters of DDANS-P1 and A-095.11 from Table 2, the main-chain polymer shows a slightly higher steepness index $m$. Polymers with larger $m$ values are found to have a broader spectrum of relaxation times (smaller stretched exponent $b$).[36] According to eq 6 of the same reference, $m$ for DDANS-P1 will be about 0.02 lower than that for A-095.11. The first data point of DDANS-P1 below $T_g$, being close to the FTH trace, indicates that the system was close to equilibrium when the decay experiment started.[52] This is equivalent to a low cooling rate. With $b = 0.19$ and a cooling rate of −0.32 K/min determined by a least-squares fit (on a logarithmic time scale) to DDANS-P1 data, the TN trace replotted in Figure 4b with WLF parameters from DDANS-P1 is in good agreement with measured relaxation times for main-chain systems.

The polyimide PI-1 ($T_g = 350$ °C) is the only case where apparently no scaling is found. Although this polymer has an impressive orientational stability at high temperatures, it shows the least-scaled stability in our comparison. A possible explanation may be similar to the one given by Weder et al.[22] that chromophore degradation is occurring at intermediate temperatures over the long period of measurement, even if a thermogravimetric analysis on a short time scale shows dye stability to much higher temperatures. The asterisk in Figure 4b illustrates this fact: a DDANS-P1 film held at 80 °C under vacuum shows a much longer relaxation time than the same material stored in air (black circles) in this intermediate temperature range.

The interpenetrating network polymer exhibits a very interesting behavior. Not only a high relaxation time of more than 500 s at $T_g$ is found but also a strong deviation from the expected scaling near $T_g$. At lower temperatures a very steep increase in relaxation time is observed. The anomalously high value extrapolated for $\tau_g$ may be a result of an increase in $T_g$ during the simultaneous poling and curing process. The effective $T_g$ measured by the SHG process may differ considerably from that inferred from the DSC measurement.

**(b) Thermorheological Simplicity and Relaxation in Nonlinear Optical Polymers.** The assumption of thermorheological simplicity (the relaxation function having the same shape at every temperature when plotted against the logarithm of time)—a condition obviously violated in SHG relaxation in NLO polymers (see Figure 12)[11,53]—is the major drawback of the TN procedure in the present form for a complete description of the relaxation mechanisms. The (fixed) stretched exponent $b \approx 0.2$ as used for the calculation of scaled SHG relaxation times is much lower than expected ($b \approx 0.5$) from the steepness index at $T_g$,[36] also lower than the values of $b$ obtained in the DSC measurements, but closer to fitted values of $b$ from the KWW fits to the SHG measurements at the lowest temperatures. The reason for this relative insensibility to the change in $b$ is that the shape of the relaxation function in eq 3.3 is not very important as long as relaxation times are shorter or of the same order of magnitude as the time scale of the experiment. Large changes in $b$ are observed mainly above and close to the glass transition, where relaxation times are short, whereas almost constant stretched exponents are found below $T_g$. Several ways of implementing thermorheological complexity have been proposed in the literature,[54−57] and work is in progress for an assessment of these theories for the description of relaxational behavior in NLO polymers.

**(c) Universality of Williams−Landel−Ferry (WLF) Parameters.** If the WLF parameters $C_1^g$ and $C_2^g$ have universal character, the steepness index is expected to be proportional to $T_g$ as given by eq 3.9. The data in Table 2 do not support this conclusion. The results from NLO polymers, however, suggest that $C_1^g$ is "more" universal, since relaxation time scaling in Figure 4 for polymers with widely differing glass transition temperatures is found and scaling as inferred from eq 3.7 is coupled to $C_1^g$ only. Data from other measurements assessing the universality of the WLF parameters are in agreement with this conclusion.[41] However, values for $C_1^g$ obtained from DSC measurements in Table 2 still vary by at least a factor of 2 from the universal WLF value of $C_1^g \approx 16$.[41] Our identification of the minimum fragility $m_{min} = C_1^g$ is therefore not consistent with a correlation of $m_{min}$ with vibrational lifetimes[36] associated with the prefactor of eq 3.1. A similar result was found by Hodge in an attempt to correlate glassy-state activation enthalpies with respect to $T_g$.[40] The previously reported data do not conclusively support the expected proportionality as implied by a constant value of $m_{min}$. This finding is also reflected in the variations in $C_1^g$ found in Table 2.

**(d) Annealing of Nonlinear Optical Polymers. Enthalpy Relaxation in Annealed Nonlinear Optical Polymers.** To test the predictive power of the TN

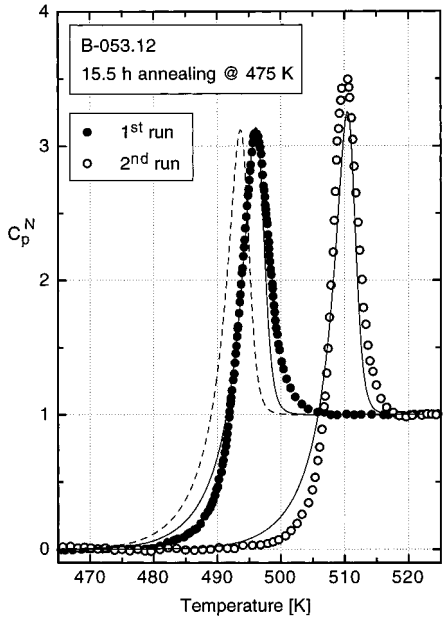


**Figure 5.** Observed shift in normalized $C_p^N$ DSC heat capacity curves of the polyimide precursor polymer B-053.12 for annealing at $T_a = 475$ K for 15.5 h. Data for the second run were taken after the measurement of the completeset of curves in Figure 6a below. To reproduce shifted DSC data (solid lines), $T_g$, $T_2$, and $T_a$ were increased by the same amount as the measured peak position temperature deviates from the model calculations with $T_g$, $T_2$, and $T_a$ taken from the unannealed sample (dashed line).

description of the glass transition for annealed probes, we performed two kinds of cyclic enthalpic recovery experiments: (1) annealing for different annealing times at a fixed annealing temperature; (2) annealing for a fixed annealing period at different annealing temperatures. We encountered two new features for these thermal histories. First, the peak of the enthalpic recovery during heating shifted its position with respect to the annealing time specifically for high overshoot data (long annealing times), and second, it was usually not possible to reproduce the same result a second time with the same sample, although each cycle was started with tempering the sample well-above the glass transition temperature (to cancel any memory effect from preceding cycles). The reason for this change in sample properties is not known, but partial chemical degradation of the chromophores during the extended heat treatment or degasing of residual solvent in the sample powder may be an explanation.

Figure 5 shows the 15.5-h annealing trace of B-053.12 together with a second run taken after all the annealing experiments shown in Figure 6a. As seen in Figure 5, the sample must have changed some of its properties during the repeated annealing cycles since it was not possible to reproduce the result of the first run. Therefore, it is also unclear to which extent the sample had already changed during the first run, as indicated by the difference from the model expectation (dashed line in Figure 5). It is interesting to note that the shifted traces of both runs can be reproduced by correcting the temperature scale ($T_g$, $T_2$, and $T_a$) by the same amount as the measured peak position temperature deviates from the model calculations with $T_g$, $T_2$, and $T_a$ taken from the unannealed sample. The same statement holds for all annealing experiments throughout this paper. We emphasize that the TN procedure naturally

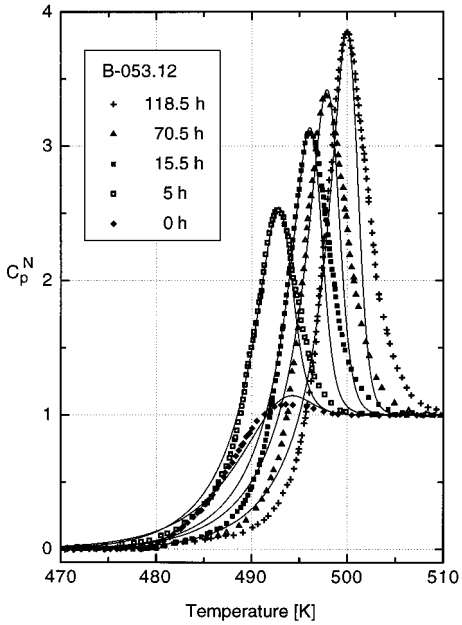


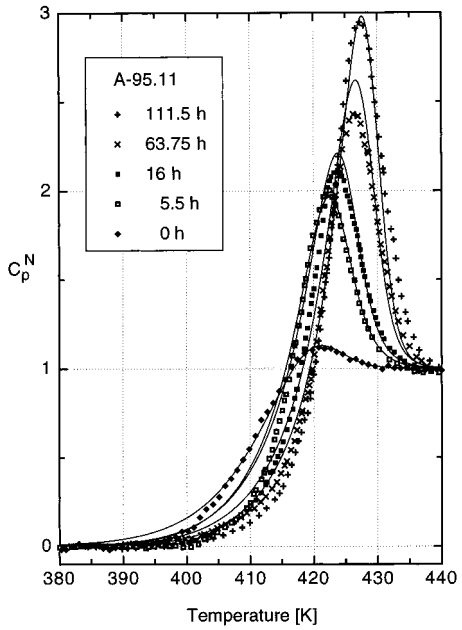


**Figure 6.** (a) Normalized $C_p^N$ DSC heat capacity curves of the polyimide precursor polymer B-053.12 for different annealing times at $T_a = 475$ K as indicated in the figure. Heating and cooling rates were all at 20 K/min. Solid lines represent peak shift corrected model expectations (see Figure 5) with enthalpic (DSC) parameters as given in Table 3. (b) As Figure 6a, for the polyimide side-chain polymer A-095.11 ($T_a = 390$ K).

cannot account for the change in material properties with sample age if parameters from experiments without annealing are used. However, shifting $T_g$ and $T_2$ by the same amount, leaving $C_2^g$ and therefore $C_1^g$ of the polymer unchanged, leads to similar results in the observed temperature range, if the temperature scale as a whole is shifted by the same amount (see eq 3.3). The fact that DSC traces can actually be calculated using this procedure strongly indicates that relevant WLF properties are not affected by aging and that the model properly incorporates the annealing step.

DSC traces from annealing experiments with different annealing times for the precursor polymer B-053.12 and

**Table 3. Enthalpic WLF Parameters Together with Glass Transition Temperature, Stretched Exponent, and Relaxation Time at the Glass Transition for the Polymers Investigated in This Work for Annealed and Unannealed Samples**

| | polymer | DDANS-P1 | A-095.11[a] | A-095.11[b] | A-148.02 | B-053.12 |
|---|---|---|---|---|---|---|
| $C_1^g$ | annealed | | 37 | 37 | 39 | 65 |
| | not annealed | 42 ± 6 | 43 ± 10 | 43 ± 10 | 40 ± 20 | 70 ± 40 |
| $C_1^g$ [K] | annealed | | 260 | 260 | 274 | 266 |
| | not annealed | 230 ± 10 | 250 ± 20 | 250 ± 20 | 270 ± 40 | 290 ± 50 |
| $T_g$ [K] | annealed | | 410 | 410 | 444 | 486 |
| | not annealed | 398 | 410 | 410 | 444 | 486 |
| $b$ | annealed | | 0.41−0.44 | 0.48 | 0.50−0.53 | 0.41−0.45 |
| | not annealed | 0.40 ± 0.02 | 0.45 ± 0.04 | 0.45 ± 0.04 | 0.50 ± 0.03 | 0.52 ± 0.09 |
| $\log(\tau_g[s]/s)$ | annealed | | 1.4 | 1.1 | 1.5 | 1.6 |
| | not annealed | 0.3 ± 0.4 | 1.7 ± 1.0 | 1.7 ± 1.0 | 1.2 ± 0.6 | 1.9 ± 0.6 |

[a] For experiments with fixed annealing temperature (see Figure 6b). [b] For experiments with fixed annealing time (see Figure 7).

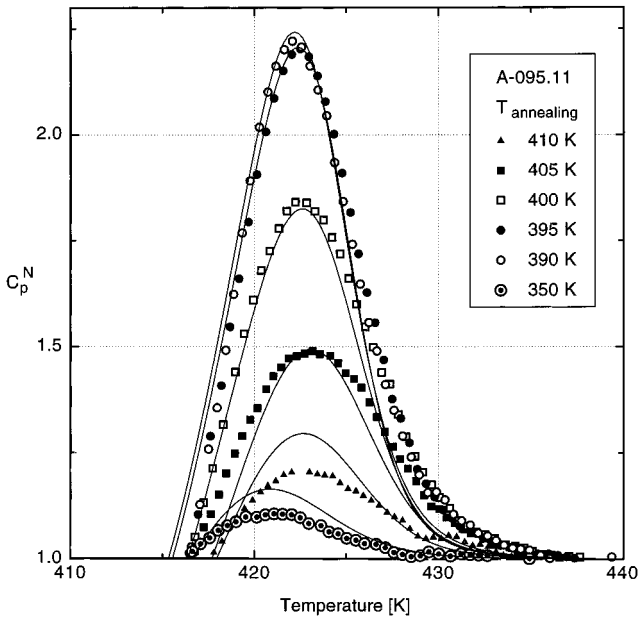


**Figure 7.** Normalized $C_p^N$ DSC heat capacity curves of the polyimide side-chain polymer A-095.11 for different annealing temperatures for a 5-h annealing as indicated in the figure. Heating and cooling rates were all at 20 K/min. Only enthalpy recovery overshoots are shown for better clarity. Solid lines represent peak shift corrected model expectations (see Figure 5) with enthalpic parameters as given in Table 3. The only parameter changed for the calculation of the different curves is the annealing temperature.

the NLO polymer A-095.11 are displayed in Figure 6a,b. Because of the peak shift, it is difficult to reproduce all thermal histories with the same parameter set $b$, $C_1^g$, $C_2^g$, $T_g$, and $\tau_g$ using eq 3.4. On the other hand it is possible to find a single parameter set that can reproduce the correct peak height of the measured curves. Calculated, peak shift corrected DSC traces in Figure 6 have been obtained by changing the annealing time and slightly adjusting $b$ in the TN procedure. The parameters used for the fits are given in Table 3. Note that all the DSC parameters for annealed samples in Table 3 are the same or within the uncertainty ranges of the averaged values from the experiments without physical aging.

The result of the second kind of experiment where the polymer A-095.11 was tempered for 5 h at different temperatures is shown in Figure 7. The condition that the measured peak height is reproduced by the TN procedure for all different annealing temperatures imposes strict constraints on the choice of the model parameters. As before, a single-parameter set was sufficient to reproduce this important feature. And again, by altering all relevant temperatures by the amount that the measured peak position temperature deviates from the model calculations with $T_g$, $T_2$, and $T_a$ taken from the unannealed sample, the measured curves are reproduced with reasonable accuracy.

We conclude that the effect of sub-$T_g$ annealing can be described by the TN procedure at least qualitatively. One major aspect, the recovery peak height, is predicted very accurately for different annealing conditions using the same single set of enthalpic (DSC) parameters as that for thermal histories without physical aging.

**Orientational Relaxation in Annealed Nonlinear Optical Polymers: Model Predictions.** On the basis of the main result of the last section (i.e., the ability to describe complex thermal histories with and without physical aging with the same WLF parameters using the TN procedure) we will develop in this section the guidelines for an optimized sample preparation procedure in order to achieve best orientational stability in NLO polymers. As was pointed out earlier,[11] orientational relaxation of the NLO susceptibility can be usefully interpreted in terms of the TN formalism using WLF parameters from dielectric (DK) measurements. Therefore, appropriate relaxation times as a function of annealing time, $t_a$, and annealing temperature, $T_a$, can be found employing the same WLF parametrization that led to the scaling result in Figure 4 in the case of no annealing. Figure 8 shows an experimental result for the increase in the relaxation time with annealing as measured by second-harmonic relaxation for the polyimide side-chain polymer A-148.02.

Keeping in mind that for temperatures far below $T_g$, an Arrhenius-type law for the relaxation times is expected with a glassy-state activation energy $E_a$ given by (cf. eq 3.5)

$$E_a \propto \frac{C_1^g C_2^g}{1 - T_2/T_{f'}} \tag{4.1}$$

where $T_{f'}$ is the final fictive temperature (relaxation times with physical aging will be determined by the respective final fictive temperature obtained during the annealing cycle). Of course, $T_{f'}$ is a function of both $t_a$ and $T_a$. Best annealing conditions are then determined by the highest activation energy achieved at the end of the annealing cycle. As an illustration, we determined optimum annealing temperatures for best orientational stability in NLO polymers at room temperature (295 K) as a function of annealing times. For this determination, we assumed that the sample is cooled at a constant rate of −5 K/min to $T_a$ and, after annealing, further cooled to room temperature at the same rate. Optimum-scaled annealing times and the expected increase in

**Table 4. Optimized Annealing Temperatures and Expected Prolongations of Second-Harmonic Relaxation Times for Physical Aging during 1 h[a]**

| polymer | $T_{a,opt}$ [K] | $\log(\tau_{SHG}/\tau_{g,SHG})$, before annealing | $\log(\tau_{SHG}/\tau_{g,SHG})$, annealing | increase in relaxation time [orders of magn.] |
|---|---|---|---|---|
| A-095.11 | 371 | 10.41 | 10.79 | 0.38 |
| DDANS-P1 | 360 | 11.30 | 11.66 | 0.36 |
| A-148.02 | 402 | 12.70 | 13.09 | 0.39 |

[a] All relaxation times are calculated at $T = 295$ K with respective WLF parameters from dielectric (DK) measurements for selected polymers. Cooling from above $T_g$ to $T_{a,opt}$ and again, after annealing, to the final temperature $T = 295$ K at a rate of −5 K/min is assumed.

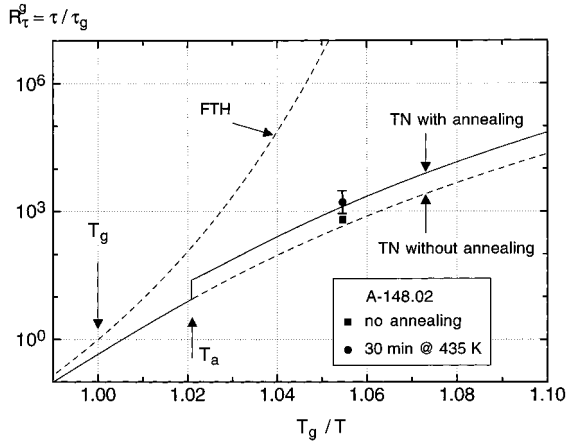


**Figure 8.** Second harmonic relaxation with annealing for the polyimide side-chain polymer A-148.02. First, the polymer film was electrode-poled above $T_g = 444$ K. Then it was cooled at $q_c = -2$ K/min to 435 K where it was annealed for $^1/_2$ h. After a renewed cooling to the decay temperature at 421 K, the poling field was turned off and the second-harmonic decay signal was collected. The solid line (TN with annealing) is the model calculation for the same thermal history, but with the FTH parameterization for A-095.11 as in Figure 4a. The scaling prediction is strongly supported by this agreement between theory and experiment. The dashed lines are the same as in Figure 4a.

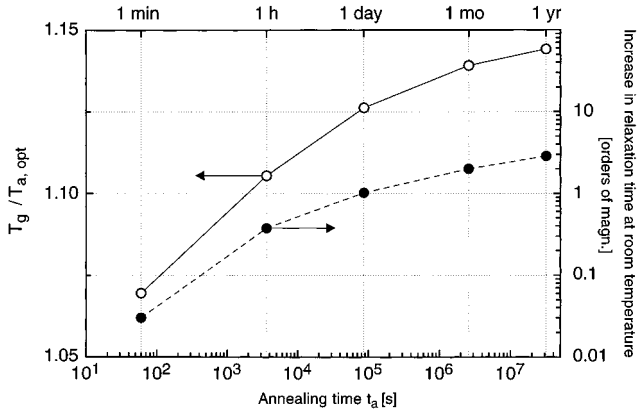


**Figure 9.** Optimum scaled annealing temperatures and increase in relaxation time for best orientational stability at room temperature (295 K) as a function of annealing time $t_a$. The thermal history assumed for the calculation is that the sample is cooled at a constant rate of 5 K/min to $T_a$ and, after annealing, further cooled to room temperature at the same rate. The TN calculations are based on WLF parameters from dielectric (DK) measurements for the polyimide side-chain polymer A-095.11.

relaxation time as a function of $t_a$ are plotted in Figure 9. The representation in a scaling graph form is justified since $T_f$, does not deviate much from $T_g$ even for $t_a$ as long as 1 year.

Table 4 compares results for A-095.11, DDANS-P1, and A-148.02 calculated with their respective WLF parameters from dielectric (DK) measurements. The very similar results again support the scaling hypothesis since tempering was performed at the same scaled annealing temperature. These results and those indicated in Figure 9 indicate that physical aging for at least 1 h is necessary to obtain a significant increase in the structural relaxation time. On the other hand, an increase of more than an order of magnitude cannot be achieved within technologically feasible annealing times.

## 5. Experiments

All experimental techniques have been described in detail in previous publications.[11,21] Here, we briefly summarize the experimental methods used in this work with examples of typical results obtained from some of our polymer samples.

**(a) Differential Scanning Calorimetry (DSC) Measurements.** DSC measurements were done on a Perkin-Elmer DSC-2C apparatus. The samples were prepared as pressed powder capsules of about 20−30 mg. A typical measurement procedure was accomplished as follows: the polymer sample was first heated to an initial temperature of about $T_g + 50$ °C for approximately 15 min. The sample was cooled at a constant rate to at least 60 °C below $T_g$ and subsequently reheated at a constant rate to the initial temperature. For the annealed samples, cooling was done at a constant rate to the annealing temperature, $T_a$, where the samples were held for the annealing time $t_a$. Afterward, the samples were further cooled to at least 60 K below $T_g$ and then reheated at a constant rate to the initial temperature. Data were always collected on the heating portion of the cycle.

The calculated heat capacity can be compared to the DSC measurement by defining the normalized heat capacity,

$$C_P^N(T) = \frac{dT_f}{dT} = \frac{C_P(T) - C_{Pg}(T)}{C_{Pe}(T) - C_{Pg}(T)} \qquad (5.1)$$

Representative DSC measurements for the polymer DDANS-P1 are shown as an example in Figure 10. The abscissa has been centered around the glass transition, which was taken according to the midpoint definition of $T_g$, $C_P^N = 0.5$.

**(b) Dielectric Measurements.** The normalized relaxation function $\phi(t)$ describing the correlation of the retarded decay of dipole moments perturbed from their equilibrium configuration by an (oscillating) external electric field is related to the frequency-dependent complex dielectric constant $\epsilon^*(w) = \epsilon'(\omega) - i\epsilon''(\omega)$ of the material by[58]

$$\frac{\epsilon^*(\omega) - \epsilon(\infty)}{\epsilon(0) - \epsilon(\infty)} = -\int_0^\infty \exp(-iuz)\, d[\exp(-u^b)] \qquad (5.2)$$

with $z = \omega\tau$ and $u = t/\tau$. The high-frequency limit is $\epsilon(\infty)$ and $\epsilon(0)$ is the DC dielectric constant. In eq 5.2 it is assumed that the relaxation $\phi(t)$ can be described by the KWW stretched exponential function, $\phi(u) = \exp(-u^b)$.

The impedance measurements were done according to the "lumped circuit" method in either a parallel or series configuration.[59] As an example, the dielectric loss curves for polymer DDANS-P1 are shown in Figure 11. The inset shows the compiled dielectric loss relaxation times together with the expected FTH behavior (see section 3).

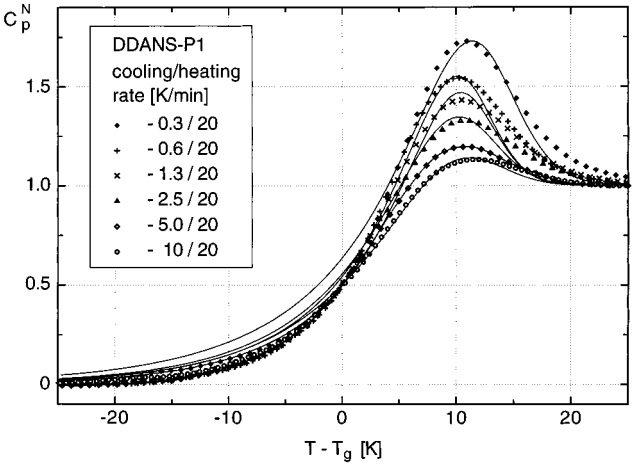


**Figure 10.** Normalized $C_p^N$ DSC heat capacity curves of the polyamide main-chain polymer DDANS-P1 for different cooling rates as indicated in the figure. A typical DSC cycle was accomplished the following way: cooling from a temperature 30 K above $T_g$ to a temperature of at least 60 K below $T_g$ followed by the heating portion of the cycle backtothe initial temperature. Data were collected on the heating portion of the cycle. All heating rates were at 20 K/min. $T_g$ is taken from the midpoint definition $C_p^N = 0.5$ of the measured data. Solid lines indicate the best fit TN calculations with enthalpic (DSC) parameters as given in Table 3.

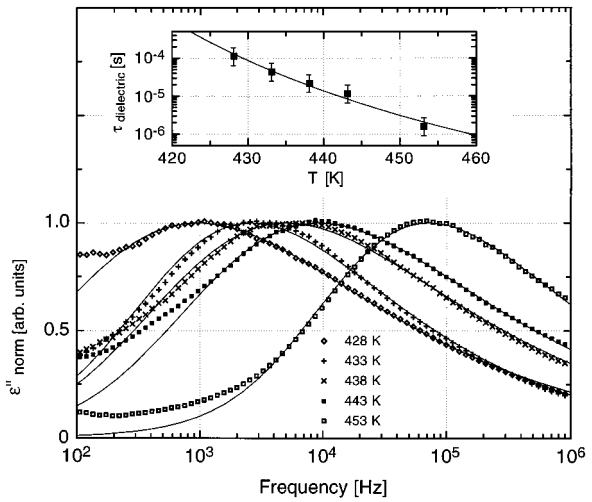


**Figure 11.** Normalized dielectric loss $\epsilon''$ frequency dependence of the polyamide main-chain polymer DDANS-P1 as a function of temperature. Solid lines give the LaPlace transform of the Kohlrausch−Williams−Watts (KWW) function. The inset shows the thus determined dielectric relaxation times, $\tau_{\text{dielectric}}$, as a function of temperature together with the expected FTH behavior (solid line).

**(c) Measurements of the Decay of Second-Harmonic Intensity.** Relaxation of the side-chain chromophores below the glass transition was investigated by the decay of the SHG signal from either corona-[3] or electrode-poled films.[9] As previously found, the time dependence of the SHG decay due to orientational relaxation (*or*) of the NLO chromophores is highly nonexponential and was also fitted to a KWW function of the form

$$d_{31}^{\text{or}}(t) = d_{31}^{\text{or}}(0) \exp -(t/\tau_{\text{or}})^b \qquad (5.3)$$

where $d_{31}$ is one of the two independent tensor elements of the nonlinear optical susceptibility of poled polymer films, assuming Kleinman and ∞-mm point group symmetry.[2] The orientational relaxation of the NLO chromophores in polymer

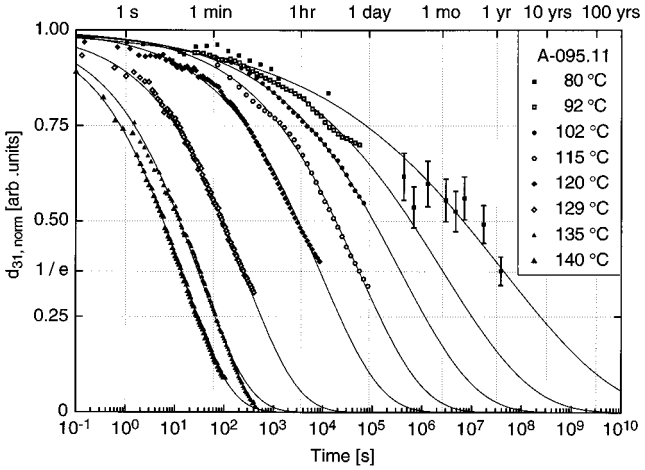


**Figure 12.** Normalized SHG relaxation for the polyimide side-chain polymer A-095.11 at different temperatures below the glass transition. Solid lines are fits to the Kohlrausch−Williams−Watts (KWW) function.

A-095.11 is plotted in Figure 12 as a function of the decay temperature.

## 6. Conclusions

We have presented orientational relaxation behavior of NLO polymers in the Tool−Narayanaswamy reduced time picture using the KWW or stretched exponential nonlinear decay function and the Adam−Gibbs expression for the relaxation time. We have shown that enthalpy relaxation and recovery can be successfully modeled by a one-parameter set for various thermal histories for samples without[11] as well as with physical aging. On the basis of these results, we introduced the WLF parametrization obtained from dielectric relaxation measurements into the model for an accurate description of SHG relaxation times in the glassy state.

Several types of NLO polymers from the literature have been compared with each other and with the polymers in this work with respect to a proposed scaling behavior with $T_g/T$ or $(T_g - T)/T$, depending on the definition of $T_g$, as the relevant scaling parameter. Scaling within side-chain and main-chain polymers is found, indicating that relaxation in these systems is governed by an increasingly larger number of cooperatively rearranging polymer segments. Guest−host-type polymers strongly deviate from scaling at temperatures far below the glass transition, an indication that the chromophore movement is decoupled from the segmental motion of the polymer backbone at temperatures far below $T_g$ in these types of polymer systems.

We have developed a model of the glass transition that allows us to analyze most of the observed thermal responses of glassy materials. Using the Tool−Narayanaswamy description of the glass transition, reformulated in a WLF parametrization, allows us to characterize the global relaxation behavior of glasses both above and below the glass transition. The model can also be applied to the calculation of relaxation times of the NLO effect due to electric-field poling. Through the model, we are able to predict the temperature and processing conditions needed to optimize the relaxational properties of poled NLO glassy polymers. The effect of sub-$T_g$ annealing, for example, is predicted to give an increase of the relaxation time by at most 1 order of magnitude for reasonable annealing times of less than 1 day.

The "strong/fragile" classification of glass formers has also been reformulated using the WLF parameters. Strong glass-forming liquids, for example, are nearly completely characterized by the WLF parameter $C_1^g$, as this determines the slope of the nearly Arrhenius behavior both above and below $T_g$. The model of the glass transition developed in this work provides an accurate means of evaluating the fragility, $m$, at the glass transition, as it describes the thermal response both above and below $T_g$. The WLF parametrization of the Tool−Narayanaswamy description of the glass transition also indicates that the minimum value of the fragility is given by $m_{min} = C_1^g$. This is inconsistent with the interpretation of the minimal fragility as being related to the vibrational bond energies, as the fitted values of $C_1^g$ to DSC data vary by at least a factor of 2, which corresponds to a variation in the vibrational bond energies of ≈20 orders of magnitude.

**Acknowledgment.** Ph. Prêtre acknowledges partial support for this work from the NSF Center on Polymer Interfaces and Macromolecular Assemblies under Award No. DMR-9400354.

## References and Notes

(1) Eich, M.; Reck, B.; Yoon, D. Y.; Willson, C. G.; Bjorklund, C. G. *J. Appl. Phys.* **1989**, *66*, 3241.
(2) Meredith, G. R.; Vandusen, J. G.; Williams, D. J. In *Nonlinear Optical Propertries of Organic and Polymeric Materials*; Williams, D. J., Eds.; ACS Symposium Series 233; Washington, DC, 1983; p 109.
(3) Mortazavi, M. A.; Knoesen, A.; Kowel, S. T.; Higgins, B. G.; Dienes, A. *J. Opt. Soc. Am. B* **1989**, *6*, 733.
(4) Singer, K. D.; Sohn, J. E.; Lalama, S. L. *Appl. Phys. Lett.* **1986**, *49*, 248.
(5) Singer, K. D.; Kuzyk, M. G.; Holland, W. R.; Sohn, J. E.; Lalama, S. J.; Comizzoli, R. B.; Katz, H. E.; Schilling, M. L. *Appl. Phys. Lett.* **1988**, *53*, 1800.
(6) Wu, J.; Valley, J. F.; Ermer, S.; Binkley, E. S.; Kenney, J. T.; Lipscomb, G. F.; Lytel, R. *Appl. Phys. Lett.* **1991**, *58*, 225.
(7) Dhinojwala, A.; Wong, G. K.; Torkelson, J. M. *Macromolecules* **1993**, *26*, 5943.
(8) Adam, G.; Gibbs, J. H. *J. Chem. Phys.* **1965**, *43*, 139.
(9) Stähelin, M.; Walsh, C. A.; Burland, D. M.; Miller, R. D.; Tweig, R. J.; Volksen, W. *J. Appl. Phys.* **1993**, *73*, 8471.
(10) Burland, D. M.; Miller, R. D.; Walsh, C. A. *Chem. Rev.* **1994**, *94*, 31.
(11) Kaatz, P.; Prêtre, P.; Meier, U.; Stalder, U.; Bosshard, C.; Günter, P.; Zysset, B.; Stähelin, M.; Ahlheim, M.; Lehr, F. *Macromolecules* **1996**, *29*, 1666.
(12) Fulcher, G. S. *J. Am. Ceram. Soc.* **1925**, *8*, 339.
(13) Williams, M. L.; Landel, R. F.; Ferry, J. D. *J. Am. Chem. Soc.* **1955**, *77*, 3701.
(14) Kovacs, A. J. *Fortschr. Hochpolym.-Fortsch.* **1963**, *3*, 394.
(15) Ferry, J. D. *Viscoelastic Properties of Polymers*, 3rd ed.; Wiley: New York, 1980.
(16) Monnerie, L. *J. Non-Cryst. Solids* **1991**, *131−133*, *755*.
(17) Tool, A. Q. *J. Am. Ceram. Soc.* **1946**, *29*, 240.
(18) Narayanaswamy, O. S. *J. Am. Ceram. Soc.* **1971**, *54*, 471.
(19) Ahlheim, M.; Lehr, F. *Makromol. Chem.* **1994**, *195*, 361.
(20) Weder, C.; Neuenschwander, P.; Suter, U. W.; Prêtre, P.; Kaatz, P.; Günter, P. *Macromolecules* **1994**, *27*, 2181.
(21) Prêtre, P.; Kaatz, P.; Bohren, A.; Günter, P.; Zysset, B.; Ahlheim, M.; Stähelin, M.; Lehr, F. *Macromolecules* **1994**, *27*, 5476.
(22) Weder, C.; Neuenschwander, P.; Suter, U. W.; Prêtre, P.; Kaatz, P.; Günter, P. *Macromolecules* **1995**, *28*, 2377.
(23) Hodge, I. M. *J. Non-Cryst. Solids* **1994**, *169*, 211.
(24) Scherer, G. W. *J. Am. Ceram. Soc.* **1984**, *67*, 504.
(25) Hodge, I. M. *Macromolecules* **1986**, *19*, 936.
(26) Moynihan, C. T.; Macedo, P. B.; Montrose, C. J.; Gupta, P. K.; DeBolt, M. A.; Dill, J. F.; Drake, P. W.; Easteal, A. J.; Elterman, P. B.; Moeller, R. P. ; Sasabe, H.; Wilder, J. A. *Ann. N.Y. Acad. Sci.* **1976**, *279*, 15.
(27) Hodge, I. M.; Berens, A. R. *Macromolecules* **1981**, *14*, 1599.
(28) Angell, C. A. *J. Res. Nat. Inst. Stand. Technol.* **1997**, *102*, 171.
(29) Moynihan, C. T.; Easteal, A. J.; DeBolt, M. A.; Tucker, J. *J. Am. Ceram. Soc.* **1976**, *59*, 12.
(30) DeBolt, M. A.; Easteal, A. J.; Macedo, P. B.; Moynihan, C. T. *J. Am. Ceram. Soc.* **1976**, *59*, 16.
(31) Hodge, I. M. *Macromolecules* **1987**, *20*, 2897.
(32) Moynihan, C. T.; Crichton, S. N.; Opalka, S. M. *J. Non-Cryst. Solids* **1991**, *131−133*, 420.
(33) Crichton, S. N.; Moynihan, C. T. *J. Non-Cryst. Solids* **1988**, *102*, 222.
(34) Sales, B. C. *J. Non-Cryst. Solids* **1990**, *119*, 136.
(35) Angell, C. A. *J. Non-Cryst. Solids* **1991**, *131−133*, 13.
(36) Böhmer, R.; Ngai, K. L.; Angell, C. A.; Plazek, D. J. *J. Chem. Phys.* **1993**, *99*, 4201.
(37) Roland, C. M.; Ngai, K. L. *J. Chem. Phys.* **1996**, *104*, 2967.
(38) Sokolov, A. P.; Kisliuk, A.; Quitmann, D.; Kudlik, A.; Rössler, E. *J. Non-Cryst. Solids* **1994**, *172−174*, 138.
(39) Vilgis, T. A. *Phys. Rev. B* **1993**, *47*, 2882.
(40) Hodge, I. M. *J. Non-Cryst. Solids* **1996**, *202*, 164.
(41) Plazek, D. J.; Ngai, K. L. *Macromolecules* **1991**, *24*, 1222.
(42) Böhmer, R.; Angell, C. A. *Phys. Rev. B* **1992**, *45*, 10091.
(43) Böhmer, R.; Angell, C. A. In *Disorder Effects on Relaxational Processes;* Richert, R., Blumen, A., Eds.; Springer-Verlag: Berlin, 1994; p 11.
(44) Chen, H. S. *Sci. Rep. Res. Inst., Tohoku Univ.* **1979**, *A27*, 97.
(45) Komatsu, T. *J. Non-Cryst. Solids* **1995**, *185*, 199.
(46) Walsh, C. A.; Burland, D. M.; Lee, V. Y.; Miller, R. D.; Smith, B. A.; Tweig, R. J.; Volksen, W. *Macromolecules* **1993**, *26*, 3720.
(47) Dhinojwala, A.; Wong, G. K.; Torkelson, J. M. *J. Chem. Phys.* **1994**, *100*, 6046.
(48) Döbler, M.; Weder, C.; Ahumada, O.; Neuenschwander, P.; Suter, U. W.; Follonier, S.; Bosshard, C.; Günter, P. *Polym. Mater. Sci. Eng.* **1997**, *76*, 308.
(49) Döbler, M.; Weder, C.; Ahumada, O.; Neuenschwander, P.; Suter, U. W.; Follonier, S.; Bosshard, C.; Günter, P. submitted to *Macromolecules*.
(50) Verbiest, T.; Burland, D. M.; Jurich, M. C.; Lee, V. Y.; Miller, R. D.; Volksen, W. *Science* **1995**, *268*, 1604.
(51) Chen, J. I.; Marturunkakul, S.; Li, L.; Jeng, R. J.; Kumar, J.; Tripathy, S. K. *Macromolecules* **1993**, *26*, 7379.
(52) Note that in this case $\tau_g$ was determined from dielectric relaxation data above in contrast to the assumption made about $\tau_g$ for PI-2 and the IPN polymer (which, of course, is based on the idea of scaling of relaxation times).
(53) Hamilton, K. E.; Torkelson, J. M. *Polym. Prepr. (Am. Chem. Soc., Div. Polym. Chem.)* **1994**, *35*, 799.
(54) Ducroux, J. P.; Rekhson, S. M.; Merat, F. L. *J. Non-Cryst. Solids* **1994**, *172−174*, 541.
(55) Matsuoka, S.; Quan, X. *Macromolecules* **1991**, *24*, 2770.
(56) Mazurin, O. V.; Startev, Y. K. *Sov. J. Glass Phys. Chem. (Eng. Trans.)* **1981**, *7*, 274.
(57) Rendell, R. W.; Ngai, K. L.; Plazek, D. J. *J. Non-Cryst. Solids* **1991**, *131−133*, 442.
(58) Williams, G. In *Comprehensive Polymer Science, Vol. 2*; Allen, G., Ed.; Pergamon Press: New York, 1989; p 311.
(59) Blythe, A. R. *Electrical Properties of Polymers;* Cambridge University Press: Cambridge, 1979.

MA9713623